SEECCM 2009
2nd South-East European Conference on Computational Mechanics
An IACM-ECCOMAS Special Interest Conference
M. Papadrakakis, M. Kojic, V. Papadopoulos (eds.)
Rhodes, Greece, 22–24 June 2009

EVALUATION STUDY OF THE IMPROVED TRIC SHELL ELEMENT FOR LINEAR AND NONLINEAR STRUCTURAL ANALYSIS

Andreas G. Gisakis*, Pavlos Tsirigas, Vagelis Plevris and Manolis Papadrakakis

Institute of Structural Analysis & Seismic Research
School of Civil Engineering
National Technical University of Athens
Zografou Campus, 15780 Athens, Greece
andreas@agisakis.gr, ptsirigas@gmail.com, {vplevris, mpapadra}@central.ntua.gr

Keywords: Shell element, Triangle, Drilling degrees, Plane stress, Benchmark tests, Natural mode.

Abstract. *The TRIC element is a simple but sophisticated three-node shear-deformable isotropic and composite facet shell element suitable for large-scale linear and nonlinear engineering computations of shell structures. The element formulation is based on the natural mode finite element method where the deformation or natural modes are separated from the rigid body modes. The element, compared to the conventional isoparametric finite element formulations, has substantial computational advantages such as analytical expressions for the computation of the stiffness matrix, as well as locking-free properties. The characteristic feature of this element is that the non-linear material behaviour is taken into account entirely on the natural coordinate system and can be expressed analytically [1,2,3].*

An evaluation study is performed of the improved TRIC element [4] in its membrane behaviour which becomes predominant in shear walls and the detailed simulation of steel structures. The enhanced features are achieved by applying an optimal method in calculating the elements of the stiffness matrix regarding the drilling degrees of freedom, while at the same time eliminating the aspect ratio locking of its predecessor. An elasto-plastic constitutive model based on the von Mises yield criterion with isotropic hardening is incorporated into the improved nonlinear TRIC shell element.

The behaviour of the element is evaluated in a number of linear and elastoplastic benchmark tests. Both the stress and displacement fields of the element are tested. The results are compared with existing analytical solutions or with numerical results obtained from commercial finite element programs. The improved element exhibits excellent performance in shell problems with significant membrane stresses and unstructured meshes, while retaining its advantages in terms of computational efficiency.

1 INTRODUCTION

An attempt to device a shell element with robustness, accuracy and efficiency has led to the derivation of the TRIC shell element [1,3], a simple but sophisticated triangular, shear-deformable facet shell element suitable for the analysis of thin and moderately thick isotropic as well as composite plate and shell structures. Its formulation is based on the natural mode finite element method [5], a method introduced by Argyris in the 1950s and then followed by many investigators, that separates the pure deformational modes -also called natural modes- from the rigid body movements of the element. The natural mode method in connection with the triangular shape of the element has substantial computational advantages compared to the conventional isoparametric finite element formulations. Appropriate treatment of the element kinematics eliminates automatically locking phenomena while all computations are performed analytically, thus avoiding the expensive numerical computation of the stiffness matrix. Furthermore, the inclusion of the transverse shear deformations in the formulation of the TRIC shell element based on a first order shear-deformable beam theory is performed in a way that eliminates the shear locking effect in a physical manner.

The TRIC element formulation can be decomposed in two different triangular elements. One for the pure-bending behavior and one for the membrane (plane stress) behavior. In a previous work [4], an enhancement of the element's membrane behavior was presented. The enhancement follows an optimal method in calculating the stiffness matrix regarding the rotational or drilling degrees of freedom (corner rotations normal to the plane of the shell element). The element performance in plane stress problems prior to the improvement was identical to that of the Constant Strain Triangle (CST) [6]. This element encounters great difficulties in determining the exact structural behavior, while it exhibits serious aspect ratio locking.

The purpose of this work is to assess via a thorough investigation the ability of the improved element to address real-world structural problems in a computationally efficient and yet accurate way in both linear and elastoplastic tests. An elasto-plastic constitutive model based on the von Mises yield criterion with isotropic hardening [7] is incorporated into the improved TRIC shell element.

2 THE TRIC ELEMENT

The formulation of the TRIC shell element has been presented thoroughly in a number of papers [1-5,7]. In the present paper, only the basic features of the element will be highlighted and particularly those that are essential for the introduced improvement.

2.1 Coordinate system of the element

The key-point for the formulation of the TRIC shell element is the adoption of the so-called natural coordinate system which has the three axes parallel to the sides of the triangle (α, β, γ). Apart from the natural system (α, β, γ) there are also the local elemental coordinate system (x', y', z') placed at the triangle's centroid, and the global Cartesian coordinate system (x, y, z). Finally, for each ply of the triangle, a material coordinate system (1, 2, 3) is defined with axis 1 being parallel to the direction of the material fibers. All four coordinate systems are depicted in Figure 1.

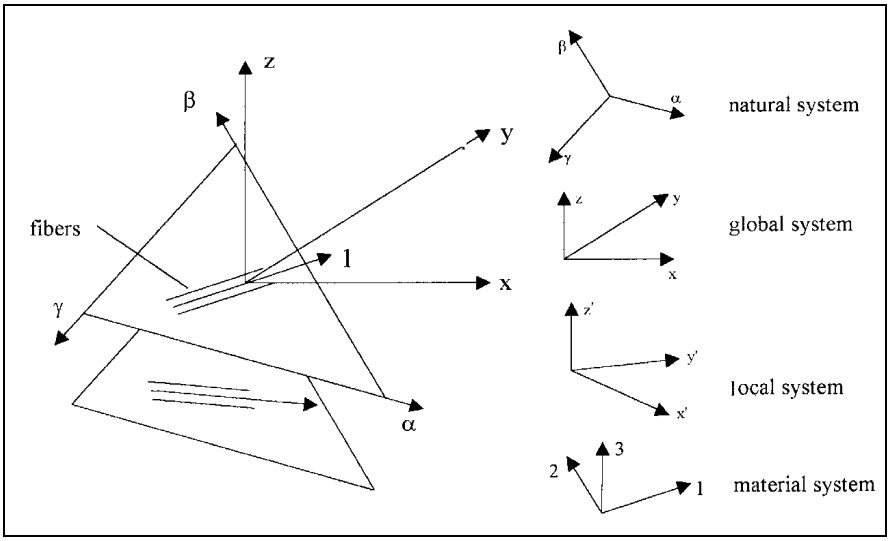

Figure 1: The multilayer triangular TRIC element: coordinate systems

2.2 From the cartesian system to the natural system – natural kinematics of the element

In the natural mode method the Cartesian strains have been replaced by the total natural strains.

$$\boldsymbol{\gamma}_t = \{\gamma_{t\alpha} \quad \gamma_{t\beta} \quad \gamma_{t\gamma}\}^T \tag{1}$$

These strains are measured directly parallel to the triangle's sides, while by definition straining of one side leaves all other triangular sides unstrained (Figure 2).

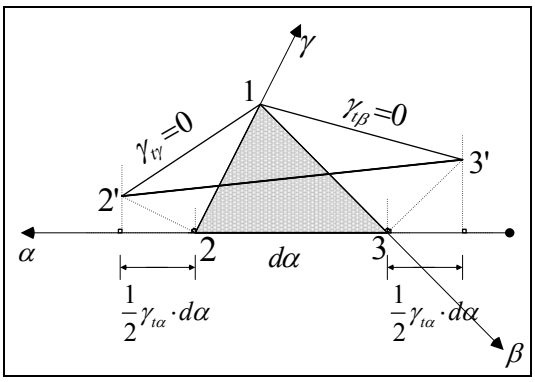

Figure 2: The total natural axial strain $\gamma_{t\alpha}$ concerning TRIC's side α.

The total natural axial strains $\boldsymbol{\gamma}_t$ are related to the three in-plane local Cartesian strains $\boldsymbol{\gamma}'$ according to the expression

$$\boldsymbol{\gamma}_t = \mathbf{B}^t\boldsymbol{\gamma}' \Leftrightarrow \begin{Bmatrix} \gamma_{t\alpha} \\ \gamma_{t\beta} \\ \gamma_{t\gamma} \end{Bmatrix} = \begin{bmatrix} c^2_{\alpha x'} & s^2_{\alpha x'} & \sqrt{2}s_{\alpha x'}c_{\alpha x'} \\ c^2_{\beta x'} & s^2_{\beta x'} & \sqrt{2}s_{\beta x'}c_{\beta x'} \\ c^2_{\gamma x'} & s^2_{\gamma x'} & \sqrt{2}s_{\gamma x'}c_{\gamma x'} \end{bmatrix} \begin{Bmatrix} \gamma_{x'x'} \\ \gamma_{y'y'} \\ \sqrt{2}\gamma_{x'y'} \end{Bmatrix} \tag{2}$$

where

$$c_{ix'} = \cos\langle i,x'\rangle \quad \text{and} \quad s_{ix'} = \sin\langle i,x'\rangle \quad \text{for} \quad i = \alpha,\beta,\gamma \tag{3}$$

and $\langle \alpha,x' \rangle, \langle \beta,x' \rangle, \langle \gamma,x' \rangle$ are the angles that the triangle's edges α, β and γ form with the local x´ axis, respectively.

The corresponding natural stresses $\boldsymbol{\sigma}_c$ to the total natural axial strains $\boldsymbol{\gamma}_t$ are grouped in the vector

$$\boldsymbol{\sigma}_c = \{\sigma_{c\alpha} \quad \sigma_{c\beta} \quad \sigma_{c\gamma}\}^T \tag{4}$$

2.3 Constitutive relations (The natural stress – strain matrix $\boldsymbol{\kappa}_{ct}$)

In the present paragraph no mention will be made to the transverse shear strains, as no modification has been made to them. With respect to the material coordinate system we will define orthotropic properties such as Young's moduli and Poisson's ratios, for every layer k, in the fashion:

$$\begin{Bmatrix} \sigma_{11} \\ \sigma_{22} \\ \sigma_{12} \end{Bmatrix}_k = \underbrace{\begin{bmatrix} \dfrac{E_1}{1-\nu_{12}\nu_{21}} & \nu_{12}\dfrac{E_1}{1-\nu_{12}\nu_{21}} & 0 \\ \nu_{12}\dfrac{E_1}{1-\nu_{12}\nu_{21}} & \dfrac{E_2}{1-\nu_{12}\nu_{21}} & 0 \\ 0 & 0 & G_{12} \end{bmatrix}_k}_{\boldsymbol{\kappa}_{12}} \begin{Bmatrix} \gamma_{11} \\ \gamma_{22} \\ \gamma_{12} \end{Bmatrix}_k \tag{5}$$

Taking into consideration that in general all material properties are temperature dependent and for complete isotropy ($\nu_{12} = \nu_{21} = \nu$, $E_1 = E_2 = E$), we come with

$$\boldsymbol{\kappa}_{12} = \frac{1}{1-\nu^2}\begin{bmatrix} E & \nu E & 0 \\ \nu E & E & 0 \\ 0 & 0 & G(1-\nu^2) \end{bmatrix}_k \quad , \quad G = \frac{E}{2(1+\nu)} \tag{6}$$

The constitutive relations between the natural stresses and the total natural strains are established by initiating the following sequence of coordinate system transformations

Material system → Local system → Natural system

With simple geometric transformations and by contemplating the invariance of the strain energy density in the different coordinate systems, one can easily reach to an expression for the constitutive matrix in the natural coordinate system for both axial and transverse deformations

$$\{\boldsymbol{\sigma}_c\}_k = [\boldsymbol{\kappa}_{ct}]\{\boldsymbol{\gamma}_t\}_k \tag{7}$$

valid for each layer k. Matrix $\boldsymbol{\kappa}_{ct}$ defines the constitutive matrices of axial straining and symmetrical bending modes. The relation between $\boldsymbol{\kappa}_{ct}$ and $\boldsymbol{\kappa}_{12}$ is given by:

$$\boldsymbol{\kappa}_{ct}{}^k = \left[\mathbf{B}^{-1}\left[\mathbf{A}^T\boldsymbol{\kappa}_{12}\mathbf{A}\right]\mathbf{B}^{-T}\right]_k \tag{8}$$

in which **A** is the transformation matrix that relates the material with the local system (its form is presented in [1]). In the present work matrix **A** is a unit vector since the material is taken as isotropic and material and local coordinate systems are identical.

2.4 Natural modes

The triangular shell element TRIC has 6 × 3 = 18 nodal displacements but only 18 - 6 = 12 independent straining modes, called natural modes, can be defined in order to satisfy all kinematic compatibility conditions. The stiffness matrix corresponding to these deformations is of dimensions 12 × 12 and is denoted as the natural stiffness matrix. A simple congruent transformation leads to the full 18 × 18 cartesian stiffness matrix of the element.

The 6 rigid-body and 12 straining natural modes (depicted in Figure 3) of the TRIC element, can be grouped in the vector $\boldsymbol{\rho}$, where $\boldsymbol{\rho}_0$ and $\boldsymbol{\rho}_N$ represent the rigid-body and straining modes, respectively:

$$\underset{(18x1)}{\boldsymbol{\rho}} = \begin{bmatrix} \underset{(6x1)}{\boldsymbol{\rho}_0} \\ \underset{(12x1)}{\boldsymbol{\rho}_N} \end{bmatrix} \qquad \boldsymbol{\rho}_0 = \begin{bmatrix} \rho_{01} & \rho_{02} & \rho_{03} & \rho_{04} & \rho_{05} & \rho_{06} \end{bmatrix}^t$$

$$\boldsymbol{\rho}_N = \begin{bmatrix} \gamma^0_{t\alpha} & \gamma^0_{t\beta} & \gamma^0_{t\gamma} & \psi_{S\alpha} & \psi_{A\alpha} & \psi_{S\beta} & \psi_{A\beta} & \psi_{S\gamma} & \psi_{A\gamma} & \psi_{\alpha} & \psi_{\beta} & \psi_{\gamma} \end{bmatrix}^t \tag{9}$$

Vector $\boldsymbol{\rho}_N$ can be subdivided in the following vectors:

$$\boldsymbol{\gamma}^0_t = \begin{bmatrix} \gamma^0_{t\alpha} & \gamma^0_{t\beta} & \gamma^0_{t\gamma} \end{bmatrix}^t \qquad \text{axial straining mode} \tag{10}$$

$$\boldsymbol{\psi}_S = \begin{bmatrix} \psi_{S\alpha} & \psi_{S\beta} & \psi_{S\gamma} \end{bmatrix}^t \qquad \text{symmetric bending mode} \tag{11}$$

$$\boldsymbol{\psi}_A = \begin{bmatrix} \psi_{A\alpha} & \psi_{A\beta} & \psi_{A\gamma} \end{bmatrix}^t \qquad \text{antisymmetric bending + shearing mode} \tag{12}$$

$$\boldsymbol{\psi}_z = \begin{bmatrix} \psi_{\alpha} & \psi_{\beta} & \psi_{\gamma} \end{bmatrix}^t \qquad \text{azimuth rotational mode} \tag{13}$$

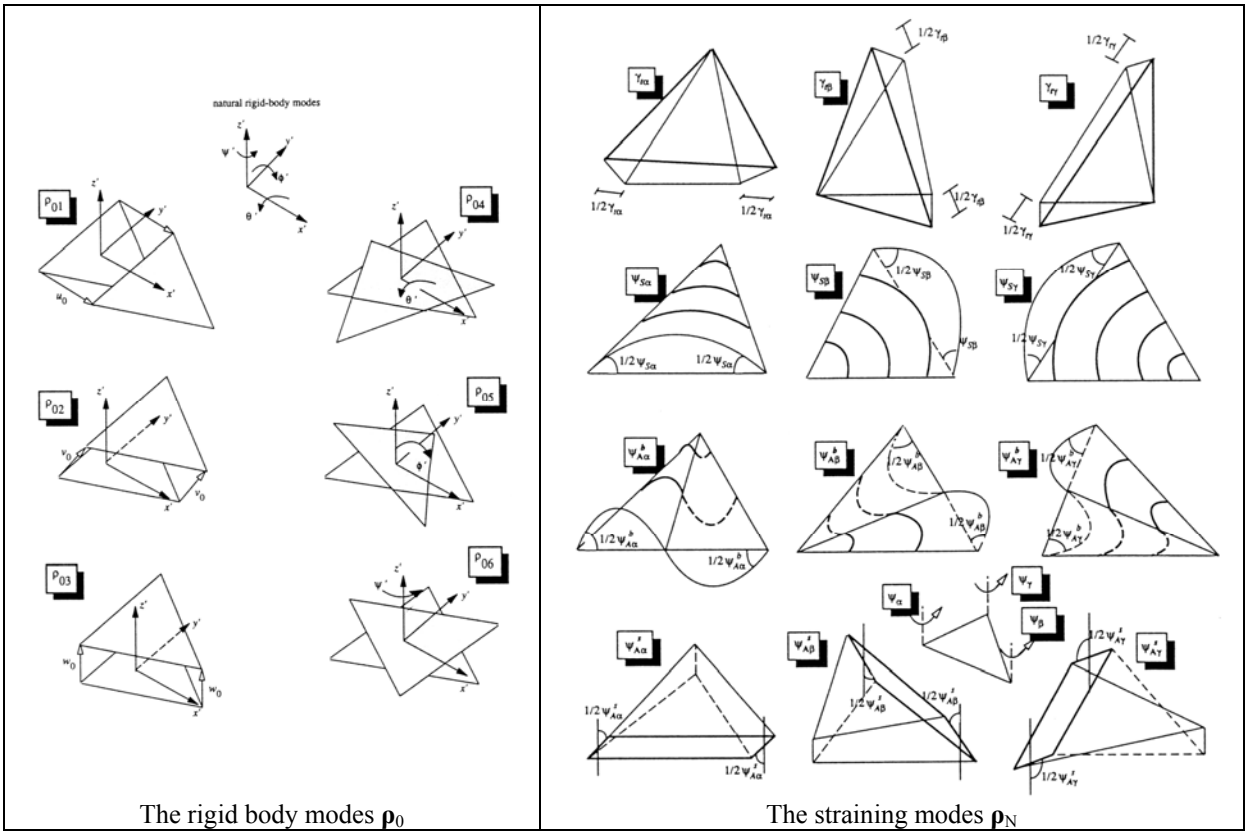

Figure 3: The Natural modes of the TRIC element

2.5 Natural stiffness matrix $\mathbf{k}_N$

The components of the natural stiffness matrix are:

$$\underset{(12\times12)}{\mathbf{k}_N} = \begin{bmatrix} \underset{(3\times3)}{\mathbf{k}_{ta}} & \mathbf{0} & \mathbf{0} \\ \mathbf{0} & \underset{(6\times6)}{\mathbf{k}_{Sq}} & \mathbf{0} \\ \mathbf{0} & \mathbf{0} & \underset{(3\times3)}{\mathbf{k}_{az}} \end{bmatrix} \tag{14}$$

where: $\mathbf{k}_{ta}$ are the axial stiffness terms, $\mathbf{k}_{Sq}$ are symmetrical bending the anti-symmetrical bending and shear stiffness terms and $\mathbf{k}_{az}$ are the stiffness terms due to in-plane rotations (azimuth stiffness terms). $\mathbf{k}_N$ is a sparse matrix of only 33 non zero entries. Since it refers to pure deformation modes, its use can provide an insight on the deformation patterns of the structure and on the ways of enhancing its performance according to the dominating straining modes. The derivation of $\mathbf{k}_{ta}$ and $\mathbf{k}_{Sq}$ was already presented in [2].

2.5.1 Azimuth stiffness matrix (initial formulation)

The drilling degrees of freedom are not involved in the derivation of the element's stiffness. However, these degrees of freedom are retained, solely for computational reasons. In the case of the TRIC element, the assignment of stiffness terms to the drilling degrees of freedom is done in a way that is consistent with the natural mode method. Three rotational springs with the same stiffness k_z are considered at the three vertices of the triangle and they are used to simulate the in-plane rotation about z' axis.

$$\mathbf{q}_{az} = \{\psi_\alpha \quad \psi_\beta \quad \psi_\gamma\}^T \tag{15}$$

The azimuth stiffness matrix $\mathbf{k}_{az}$ is then calculated as:

$$\mathbf{k}_{az} = k_z \begin{bmatrix} 1 & -0.5 & -0.5 \\ -0.5 & 1 & -0.5 \\ -0.5 & -0.5 & 1 \end{bmatrix} \tag{16}$$

with k_z having an arbitrary but small enough value, compared to the rest of the stiffness terms, so that it will produce a negligible effect on the final equilibrium equations.

$$k_z = 10^{-6}\Omega \times max\left\{ \frac{1}{l_\alpha^{\,2}} \int_{-h/2}^{h/2} z^2 k_{\alpha\alpha} dz \;,\; \frac{1}{l_\beta^{\,2}} \int_{-h/2}^{h/2} z^2 k_{\beta\beta} dz \;,\; \frac{1}{l_\gamma^{\,2}} \int_{-h/2}^{h/2} z^2 k_{\gamma\gamma} dz \right\} \tag{17}$$

where h is the thickness of the shell element, l_i $(i = \alpha, \beta, \gamma)$ are the lengths of the three sides of the element, Ω is the element area and $k_{\alpha\alpha}$, $k_{\beta\beta}$, $k_{\gamma\gamma}$ are the diagonal terms of $\boldsymbol{\kappa}_{ct}$.

2.6 The Global cartesian stiffness matrix $\bar{\mathbf{k}}$

The cartesian stiffness matrix $\mathbf{k}$ in the local coordinate system can be found using the following transformation:

$$\underset{(18\times18)}{\mathbf{k}} = \underset{(18\times12)}{\bar{\boldsymbol{\alpha}}_N^T} \; \underset{(12\times12)}{\mathbf{k}_N} \; \underset{(12\times18)}{\bar{\boldsymbol{\alpha}}_N} \tag{18}$$

where $\bar{\boldsymbol{\alpha}}_{\mathrm{N}}$ is the matrix that relates the natural straining modes $\boldsymbol{\rho}_{\mathrm{N}}$ to the Cartesian nodal displacements $\bar{\boldsymbol{\rho}}$

$$\underset{(1\times 18)}{\bar{\boldsymbol{\rho}}^{\mathrm{T}}} = \left[u' \quad \upsilon' \quad w' \quad \theta' \quad \phi' \quad \psi'\right]_i^{\mathrm{T}} \qquad i = 1,2,3 \tag{19}$$

with u_i, υ_i, w_i being the three nodal translations and θ_i, φ_i, ψ_i the three nodal rotations of node i.

$$\boldsymbol{\rho}_{\mathrm{N}} = \bar{\boldsymbol{\alpha}}_{\mathrm{N}} \bar{\boldsymbol{\rho}} \tag{20}$$

The calculation of $\bar{\boldsymbol{\alpha}}_{\mathrm{N}}$ is done using strictly geometrical arguments and can be expressed analytically. In the case of total natural axial strains $\boldsymbol{\gamma}_{\mathbf{t}}$ the relation to the Cartesian nodal displacements $\bar{\boldsymbol{\rho}}$ can de easily deducted from Figure 3 as:

$$\gamma_{t\alpha} = \frac{x_\alpha}{l_\alpha^2}(u_3 - u_2) + \frac{y_\alpha}{l_\alpha^2}(\upsilon_3 - \upsilon_2)\,,\ \gamma_{t\beta} = \frac{x_\beta}{l_\beta^2}(u_1 - u_3) + \frac{y_\beta}{l_\beta^2}(\upsilon_1 - \upsilon_3)\,,\ \gamma_{t\gamma} = \frac{x_\gamma}{l_\gamma^2}(u_2 - u_1) + \frac{y_\gamma}{l_\gamma^2}(\upsilon_2 - \upsilon_1) \tag{21}$$

while x_i, y_i $(i = \alpha, \beta, \gamma)$ is the projection of the element's sides in global coordinate axis x and y respectively and l_i is the length of the element's sides.

A final transformation leads to the global elemental stiffness $\bar{\mathbf{k}}_{(18\times 18)}$

$$\underset{(18\times 18)}{\bar{\mathbf{k}}} = \underset{(18\times 18)}{\mathbf{T}_{06}^{\mathrm{T}}}\ \underset{(18\times 18)}{\mathbf{k}}\ \underset{(18\times 18)}{\mathbf{T}_{06}} \tag{22}$$

where $\mathbf{T}_{06}$ is a hyper diagonal matrix consisted of direction cosines formed between the local and the global Cartesian coordinate system according to Figure 1. Details concerning the element's full natural and Cartesian stiffness matrices are given in [1].

3 THE CONTINUUM ELASTO-PLASTIC CONSTITUTIVE MATRIX [7]

The natural elasto-plastic stiffness of the TRIC shell element has the same structure as the natural elastic stiffness. If we ignore the influence of the shearing stresses on the elasto-plastic behaviour of the element, we only have to express eq.(7) in incremental form and replace the natural elastic material stiffness $\boldsymbol{\kappa}_{\mathrm{ct}}^{\mathrm{el}}$ by the natural elasto-plastic material stiffness $\boldsymbol{\kappa}_{\mathrm{ct}}^{\mathrm{el\text{-}pl}}$ [8,9]. In this case the components of antisymmetric stiffness $\mathrm{k_A}$ remain elastic. The primary objective in this section is to establish the explicit form of the relation between the natural strain and stress increments for each layer r within a given load step:

$$\mathrm{d}\boldsymbol{\sigma}_{\mathrm{c}}^{\mathrm{r}} = \boldsymbol{\kappa}_{\mathrm{ct}}^{\mathrm{el-pl}}\,\mathrm{d}\boldsymbol{\gamma}_{\mathrm{t}}^{\mathrm{r}} \tag{23}$$

In the following discussion the superscript r is omitted for convenience.

We start with the assumption that the total natural strain increment $\mathrm{d}\boldsymbol{\gamma}_{\mathrm{t}}$ is the sum of $\mathrm{d}\boldsymbol{\gamma}_{\mathrm{t}}^{\mathrm{el}}$, representing the elastic component of the strain, and the $\mathrm{d}\boldsymbol{\gamma}_{\mathrm{t}}^{\mathrm{pl}}$ representing the irreversible plastic component of the strain:

$$\mathrm{d}\boldsymbol{\gamma}_{\mathrm{t}} = \mathrm{d}\boldsymbol{\gamma}_{\mathrm{t}}^{\mathrm{el}} + \mathrm{d}\boldsymbol{\gamma}_{\mathrm{t}}^{\mathrm{pl}} \tag{24}$$

The stress increment follows then as

$$\mathrm{d}\boldsymbol{\sigma}_{\mathrm{c}} = \boldsymbol{\kappa}_{\mathrm{ct}}^{\mathrm{el}}\,\mathrm{d}\boldsymbol{\gamma}_{\mathrm{t}} - \boldsymbol{\kappa}_{\mathrm{ct}}^{\mathrm{el}}\,\mathrm{d}\boldsymbol{\gamma}_{\mathrm{t}}^{\mathrm{pl}} \tag{25}$$

the elastic natural strain increment is calculated as

$$\mathrm{d}\boldsymbol{\gamma}_{\mathrm{t}}^{\mathrm{el}} = \left[\boldsymbol{\kappa}_{\mathrm{ct}}^{\mathrm{el}}\right]^{-1} \mathrm{d}\boldsymbol{\sigma}_{\mathrm{c}} \tag{26}$$

where $\mathrm{d}\boldsymbol{\sigma}_{\mathrm{c}}$ is the incremental natural stress vector and $\boldsymbol{\kappa}_{\mathrm{ct}}^{\mathrm{el}}$ is the elastic constitutive matrix. In this formulation, it is assumed that the material is isotropic.

The incremental natural plastic strain is given by the following equation:

$$\mathrm{d}\boldsymbol{\gamma}_{\mathrm{t}}^{\mathrm{pl}} = \mathrm{d}\bar{\gamma}_{\mathrm{t}}^{\mathrm{pl}} \mathbf{s}_{\mathrm{N}} \tag{27}$$

where $\mathbf{s}_{\mathrm{N}}$ is a vector which determines the direction of the $\mathrm{d}\boldsymbol{\gamma}_{\mathrm{t}}^{\mathrm{pl}}$ and is defined by the normality flow rule as

$$\mathbf{s}_{\mathrm{N}} = \frac{\partial \mathrm{F}}{\partial \boldsymbol{\sigma}_{\mathrm{c}}} = \left[\frac{\partial \mathrm{F}}{\partial \sigma_{\mathrm{c}\alpha}} \quad \frac{\partial \mathrm{F}}{\partial \sigma_{\mathrm{c}\beta}} \quad \frac{\partial \mathrm{F}}{\partial \sigma_{\mathrm{c}\gamma}} \right]^{\mathrm{t}} \tag{28}$$

in which F is the yield criterion given in terms of natural stress $\boldsymbol{\sigma}_{\mathrm{c}}$, and $\mathrm{d}\bar{\gamma}_{\mathrm{t}}^{\mathrm{pl}}$ is a positive constant, the so-called equivalent plastic strain increment.

Using the above equations, the total strain increment $\mathrm{d}\boldsymbol{\gamma}_{\mathrm{t}}$ can be written as

$$\mathrm{d}\boldsymbol{\gamma}_{\mathrm{t}} = \left[\boldsymbol{\kappa}_{\mathrm{ct}}^{\mathrm{el}}\right]^{-1} \mathrm{d}\boldsymbol{\sigma}_{\mathrm{c}} + \mathrm{d}\bar{\gamma}_{\mathrm{t}}^{\mathrm{pl}} \mathbf{s}_{\mathrm{N}} \tag{29}$$

and $\mathrm{d}\boldsymbol{\sigma}_{\mathrm{c}}$ as

$$\mathrm{d}\boldsymbol{\sigma}_{\mathrm{c}} = \left[\boldsymbol{\kappa}_{\mathrm{ct}}^{\mathrm{el}}\right] \mathrm{d}\boldsymbol{\gamma}_{\mathrm{t}} - \mathrm{d}\bar{\gamma}_{\mathrm{t}}^{\mathrm{pl}} \left[\boldsymbol{\kappa}_{\mathrm{ct}}^{\mathrm{el}}\right] \mathbf{s}_{\mathrm{N}} \tag{30}$$

In case of von Mises yield condition, the yield surface may be expressed as

$$\mathrm{F}(\boldsymbol{\sigma}_{\mathrm{c}}, \bar{\gamma}_{\mathrm{t}}^{\mathrm{pl}}) = \bar{\sigma} - \sigma_{\mathrm{y}}(\bar{\gamma}_{\mathrm{t}}^{\mathrm{pl}}) = 0 \tag{31}$$

where $\bar{\sigma}$ is the equivalent stress and σ_{y} is the yield stress. The equivalent stress is derived in the next section and is defined explicitly by

$$\bar{\sigma}^2 = \frac{3}{2} \boldsymbol{\sigma}_{\mathrm{c}}^{\mathrm{t}} \left[\mathbf{A} - \frac{1}{3} \mathbf{E}_3 \right] \boldsymbol{\sigma}_{\mathrm{c}} \tag{32}$$

where

$$\mathbf{E}_3 = \begin{bmatrix} 1 & 1 & 1 \\ 1 & 1 & 1 \\ 1 & 1 & 1 \end{bmatrix} \quad , \quad \mathbf{A} = \begin{bmatrix} 1 & \cos^2\alpha & \cos^2\beta \\ \cos^2\alpha & 1 & \cos^2\gamma \\ \cos^2\beta & \cos^2\gamma & 1 \end{bmatrix} \tag{33}$$

and α, β, γ are the angles of the triangle.

Differentiating the yield criterion, gives:

$$\begin{aligned} \mathrm{dF}(\boldsymbol{\sigma}_{\mathrm{c}}, \bar{\gamma}_{\mathrm{t}}^{\mathrm{pl}}) = \mathrm{d}(\bar{\sigma} - \sigma_{\mathrm{y}}(\bar{\gamma}_{\mathrm{t}}^{\mathrm{pl}})) &= \frac{\partial(\bar{\sigma} - \sigma_{\mathrm{y}}(\bar{\gamma}_{\mathrm{t}}^{\mathrm{pl}}))}{\partial \boldsymbol{\sigma}_{\mathrm{c}}} \mathrm{d}\boldsymbol{\sigma}_{\mathrm{c}} + \frac{\partial(\bar{\sigma} - \sigma_{\mathrm{y}}(\bar{\gamma}_{\mathrm{t}}^{\mathrm{pl}}))}{\partial \bar{\gamma}_{\mathrm{t}}^{\mathrm{pl}}} \mathrm{d}\bar{\gamma}_{\mathrm{t}}^{\mathrm{pl}} = 0 \\ &= \mathbf{s}_{\mathrm{N}}^{\mathrm{t}} \mathrm{d}\boldsymbol{\sigma}_{\mathrm{c}} - \mathrm{H} \mathrm{d}\bar{\gamma}_{\mathrm{t}}^{\mathrm{pl}} = 0 \end{aligned} \tag{34}$$

where

$$H = -\frac{\partial(\bar{\sigma} - \sigma_y(\bar{\gamma}_t^{pl}))}{\partial \bar{\gamma}_t^{pl}} \tag{35}$$

H is the hardening modulus and in our case is defined as

$$H = \frac{d\boldsymbol{\sigma}_c}{d\bar{\gamma}_t^{pl}}, \quad \sigma_c > \sigma_y \tag{36}$$

From the yield condition the equivalent plastic strain increment is derived as

$$d\bar{\gamma}_t^{pl} = \frac{1}{H}\mathbf{s}_N^t d\boldsymbol{\sigma}_c \geq 0 \tag{37}$$

Alternatively, the equivalent plastic strain can be expressed in terms of the strain increments by substituting (27) and (30) in (37):

$$d\bar{\gamma}_t^{pl} = \frac{1}{H + \mathbf{s}_N^t \boldsymbol{\kappa}_{ct}^{el} \mathbf{s}_N} \mathbf{s}_N^t \boldsymbol{\kappa}_{ct}^{el} d\boldsymbol{\gamma}_t \geq 0 \tag{38}$$

Finally, after substitution of (27), (38) in (30) we obtain (23) in explicit form

$$d\boldsymbol{\sigma}_c^r = \left[\boldsymbol{\kappa}_{ct}^{el} - \frac{1}{H + \mathbf{s}_N^t \boldsymbol{\kappa}_{ct}^{el} \mathbf{s}_N} (\boldsymbol{\kappa}_{ct}^{el} \mathbf{s}_N)(\boldsymbol{\kappa}_{ct}^{el} \mathbf{s}_N)^t \right]^r d\boldsymbol{\gamma}_t^r \tag{39}$$

where the expression in brackets corresponds to the standard continuum elasto-plastic material stiffness matrix $\boldsymbol{\kappa}_{ct}^{el-pl}$ valid for every layer r:

$$[\boldsymbol{\kappa}_{ct}^{el-pl}]^r = \left[\boldsymbol{\kappa}_{ct}^{el} - \frac{1}{H + \mathbf{s}_N^t \boldsymbol{\kappa}_{ct}^{el} \mathbf{s}_N} (\boldsymbol{\kappa}_{ct}^{el} \mathbf{s}_N)(\boldsymbol{\kappa}_{ct}^{el} \mathbf{s}_N)^t \right]^r \tag{40}$$

The criterion for the existence of elasto-plastic natural matrix is obviously the equivalent plastic strain increment $d\bar{\gamma}_t^{pl}$ which is greater than zero only if plastic yielding takes place. The natural strain increment in the r-th layer $d\boldsymbol{\gamma}_t^r$ which is used as input to (39) is related to the components $d\gamma_{ti}^0$ and $d\psi_{Si}$ of the incremental natural modes vector $d\boldsymbol{\rho}_N$:

$$d\gamma_{ti}^r = d\gamma_{ti}^0 + z_r' \frac{d\psi_{Si}}{l_i}, \quad i = \alpha, \beta, \gamma \tag{41}$$

The natural elasto-plastic stiffness of the element is obtained by summing up the natural elasto-plastic layer stiffnesses of the element. Following the expression for the natural elastic stiffness matrix, the elasto-plastic one is given by

$$\mathbf{k}_N^{el-pl} = \sum_{r=1}^{nl} \left(\boldsymbol{\alpha}_N^t \boldsymbol{\kappa}_{ct}^{el-pl} \boldsymbol{\alpha}_N \right) \tag{42}$$

where nl is the number of layers.

4 IMPROVEMENT OF THE MEMBRANE BEHAVIOR

The improvements presented in this work are inspired by the work of Felippa and co-workers [10-13]. In their study an optimal 9-dof plane stress triangular element is designed based on the on the Assumed Natural Deviatoric Strain (ANDES) formulation, a variant of the assumed natural strain (ANS) formulation. The key concept of ANDES is that only the deviatoric part of the strains is assumed over the element, whereas the mean strain part is discarded in favor of a constant stress assumption.

4.1 Drilling degrees of freedom

The drilling degrees of freedom are useful for compactly expressing the higher order behavior of the element. The azimuth corner rotations

$$\boldsymbol{\psi}_z = \begin{Bmatrix} \psi_\alpha & \psi_\beta & \psi_\gamma \end{Bmatrix}^T \tag{43}$$

are extracted from the total corner rotations ψ_z^{total}, subtracting the mean or CST rotation ρ_{06}:

$$\psi_z = \psi_z^{\text{total}} - \rho_{06} \tag{44}$$

where $z = \alpha, \beta, \gamma$ and

$$\rho_{06} = \frac{1}{4\Omega}(x_\alpha u_1 + x_\beta u_2 + x_\gamma u_3 + y_\alpha v_1 + y_\beta v_2 + y_\gamma v_3) \tag{45}$$

is the geometric expression that relates the nodal translational degrees of freedom with the 6th natural rigid-body mode ρ_{06}.

4.2 Azimuth stiffness matrix $\mathbf{k}_{az}$ (modification)

The modified azimuth stiffness matrix is given by

$$\underset{(3\times3)}{\mathbf{k}_{az}} = \sum_{k=1,2,..,nl} \underset{(3\times3)}{\mathbf{k}_\psi^k} \tag{46}$$

where $\mathbf{k}_\psi^k$ is the azimuth stiffness matrix in each layer (k) of the element in terms of the azimuth corner rotations ψ_z of eq. (44).

To express $\mathbf{k}_\psi^k$ compactly, the following matrices are introduced, which depend on nine free dimensionless parameters, β_1 through β_9

$$\mathbf{Q}_1 = \frac{2\Omega}{3}\begin{bmatrix} \frac{\beta_4}{l_a^2} & \frac{\beta_5}{l_a^2} & \frac{\beta_6}{l_a^2} \\ \frac{\beta_7}{l_\beta^2} & \frac{\beta_8}{l_\beta^2} & \frac{\beta_9}{l_\beta^2} \\ \frac{\beta_1}{l_\gamma^2} & \frac{\beta_2}{l_\gamma^2} & \frac{\beta_3}{l_\gamma^2} \end{bmatrix}, \quad \mathbf{Q}_2 = \frac{2\Omega}{3}\begin{bmatrix} \frac{\beta_3}{l_a^2} & \frac{\beta_1}{l_a^2} & \frac{\beta_2}{l_a^2} \\ \frac{\beta_6}{l_\beta^2} & \frac{\beta_4}{l_\beta^2} & \frac{\beta_5}{l_\beta^2} \\ \frac{\beta_9}{l_\gamma^2} & \frac{\beta_7}{l_\gamma^2} & \frac{\beta_8}{l_\gamma^2} \end{bmatrix}, \quad \mathbf{Q}_3 = \frac{2\Omega}{3}\begin{bmatrix} \frac{\beta_8}{l_a^2} & \frac{\beta_9}{l_a^2} & \frac{\beta_7}{l_a^2} \\ \frac{\beta_3}{l_\beta^2} & \frac{\beta_1}{l_\beta^2} & \frac{\beta_2}{l_\beta^2} \\ \frac{\beta_5}{l_\gamma^2} & \frac{\beta_6}{l_\gamma^2} & \frac{\beta_4}{l_\gamma^2} \end{bmatrix} \tag{47}$$

Matrix $\mathbf{Q}_i$ relates the natural strains $\boldsymbol{\gamma}_t$, at elements corner *i*, to the azimuth corner rotations $\boldsymbol{\psi}_Z$. At any point of triangular coordinates $\{\zeta_1, \zeta_2, \zeta_3\}$

$$\boldsymbol{\gamma}_t = \mathbf{Q}\boldsymbol{\psi}_z \tag{48}$$

where

$$\mathbf{Q}=\mathbf{Q}_1\zeta_1 + \mathbf{Q}_2\zeta_2 + \mathbf{Q}_3\zeta_3 \tag{49}$$

If we evaluate eq. (48) and eq. (49) at the midpoints we get:

$$\mathbf{Q}_4 = \frac{1}{2}(\mathbf{Q}_1 + \mathbf{Q}_2)\,, \quad \mathbf{Q}_5 = \frac{1}{2}(\mathbf{Q}_2 + \mathbf{Q}_3)\,, \quad \mathbf{Q}_6 = \frac{1}{2}(\mathbf{Q}_3 + \mathbf{Q}_1) \tag{50}$$

Finally:

$$\mathbf{k}_{\psi}^{k}=h(\mathbf{Q}_4^{T}\boldsymbol{\kappa}_{ct}\mathbf{Q}_4+\mathbf{Q}_5^{T}\boldsymbol{\kappa}_{ct}\mathbf{Q}_5 + \mathbf{Q}_6^{T}\boldsymbol{\kappa}_{ct}\mathbf{Q}_6) \tag{51}$$

and

$$\mathbf{k}_{az}^{k} = \frac{3}{4}\beta_0\mathbf{k}_{\psi}^{k} \tag{52}$$

where β_0 is an overall scaling coefficient. This coefficient could be absorbed into the β_1 through β_9 but it is left separate, to simplify the incorporation of material behavior into eq. (51). The factor ¾ comes from "historical grandfathering" [10].

The free dimensionless parameters β_i are determined from a higher order patch test which tunes up the higher order stiffness of triangular elements. Using such a patch test the optimal parameters are calculated as follows:

$$\beta_0 = \frac{1}{2}(1 - 4\nu^2), \beta_1 = 1, \beta_2 = 2, \beta_3 = 1, \beta_4 = 0, \beta_5 = 1, \beta_6 = -1, \beta_7 = -1, \beta_8 = -1, \beta_9 = -2 \tag{53}$$

Since for v = ½ the optimal β_0 is 0, the azimuth stiffness would vanish and the element is rank deficient. To maintain stability β_0 is set to a minimum value, for example

$$\beta_0 = \max\left(\frac{(1 - 4\nu^2)}{2},\ 0.01\right) \tag{54}$$

4.3 Cartesian stiffness matrix k (modification)

So far we focused our attention on the calculation of the stiffness terms of azimuth modes in the natural system. It remains to establish the relation between the azimuth modes in the natural and in the local systems. Furthermore it should be noted that in the basic TRIC element the coupling terms of eq. (14), connecting these degrees of freedom with the rest of the modes were set equal to zero. This means that there is no coupling of the axial, symmetric bending, antisymmetric bending and shearing modes when the element is distorted in the azimuthian direction.

In section 2.6 it was shown that the Cartesian stiffness matrix **k** in the local coordinate system can be found using eq. (18), and $\bar{\boldsymbol{\alpha}}_N$ is the matrix that relates the natural straining modes $\boldsymbol{\rho}_N$ to the Cartesian nodal displacements $\bar{\boldsymbol{\rho}}$. Therefore $\bar{\boldsymbol{\alpha}}_N$ is solely a function of the current geometry of the element and is derived based upon pure geometrical relations between $\boldsymbol{\rho}_N$ and $\bar{\boldsymbol{\rho}}$. This matrix can now be used to produce all the above mentioned geometric expressions.

4.3.1 Relation between the azimuth modes in the natural and in the local system

By applying eq. (44) and eq. (45) to the three corners we assemble the transformation:

$$\boldsymbol{\psi}_Z = \begin{Bmatrix} \psi_\alpha \\ \psi_\beta \\ \psi_\gamma \end{Bmatrix} = \frac{1}{4\Omega} \begin{bmatrix} x_a & y_a & 4\Omega & x_\beta & y_\beta & 0 & x_\gamma & y_\gamma & 0 \\ x_a & y_a & 0 & x_\beta & y_\beta & 4\Omega & x_\gamma & y_\gamma & 0 \\ x_a & y_a & 0 & x_\beta & y_\beta & 0 & x_\gamma & y_\gamma & 4\Omega \end{bmatrix} \begin{Bmatrix} u_i' \\ v_i' \\ \psi_i' \end{Bmatrix}_{i=1,2,3} \tag{55}$$

In the above eq. we present only those elements of $\bar{\boldsymbol{\rho}}$ that have a relation with $\boldsymbol{\psi}_z$. All other degrees of freedom (w_i, θ_i, ϕ_i, where $i=1,2,3$) have columns equal to zero in the above transformation matrix. This relationship was incorporated in the basic TRIC theory [1], but due to the arbitrary and small value of matrix $\mathbf{k}_{az}$ (eq. (16)) in $\mathbf{k}_N$ (eq. (14)) its influence was negligible.

The second modification deals with the coupling terms in eq. (14). According to the basic TRIC theory the natural axial straining modes are related only with the in-plane local deformation degrees of freedom (u_i', v_i' for i=1,2,3). However, these modes are also causing a distortion to the element angles. This distortion can be expressed as:

$$\begin{Bmatrix} \gamma_{t\alpha} \\ \gamma_{t\beta} \\ \gamma_{t\gamma} \end{Bmatrix} = \frac{a_b h}{12} \begin{bmatrix} y_a(y_b - y_\gamma) & x_a(x_b - x_\gamma) & 2(y_b x_b - y_\gamma x_\gamma) \\ y_\beta(y_\gamma - y_\alpha) & x_\beta(x_\gamma - x_\alpha) & 2(y_\gamma x_\gamma - y_\alpha x_\alpha) \\ y_\gamma(y_\alpha - y_\beta) & x_\gamma(x_\alpha - x_\beta) & 2(y_\alpha x_\alpha - y_\beta x_\beta) \end{bmatrix} \mathbf{B} \begin{Bmatrix} \psi_1' \\ \psi_2' \\ \psi_3' \end{Bmatrix} \Leftrightarrow \boldsymbol{\gamma}_t = \frac{a_b h}{12} \mathbf{L}\mathbf{B}\boldsymbol{\psi}_i' \tag{56}$$

where h is the element's height, $\mathbf{B}$ is given in eq. (2) and $\mathbf{L}$ is the lumping matrix [10] which expresses the relationship between the nodal forces produced by constant-strain modes and an arbitrary constant-stress field ($\mathbf{t}_c = \mathbf{L}\boldsymbol{\sigma}_c$). The matrix $\mathbf{L}$ is a (9x3) matrix which relates the natural axial straining modes with both the 6 in plane translations and the 3 azimuthian rotations of the element. In the present modification, this matrix is used only for the coupling terms between the natural axial straining modes and the 3 azimuthian rotations of the element. That is the reason why only a (3x3) lumping matrix is presented in eq. (56).

Finally α_b is a variable which controls the amount of the element angle distortion. An examination of α_b shows that, if it is set equal to zero we return to the basic theory, if it is set greater than 1 the element will have large rotational stiffness. The value of α_b should always be in the range of 1 thought 2 and is not sensitive to the choice of material properties. Its value depends only the elements geometry and on the elements corners (3 different α_b for every corner). The average value α_b=*1.5* is recommended for general use in arbitrary meshes [10].

Using eq. (56) we get:

$$\frac{a_b h}{12}\mathbf{L}\mathbf{B} = \begin{bmatrix} 0 & \frac{\Omega}{2l_a^2} & -\frac{\Omega}{2l_a^2} \\ -\frac{\Omega}{2l_\beta^2} & 0 & \frac{\Omega}{2l_\beta^2} \\ \frac{\Omega}{2l_\gamma^2} & -\frac{\Omega}{2l_\gamma^2} & 0 \end{bmatrix} \tag{57}$$

and eq. (21) then becomes:

$$\gamma_{t\alpha} = \frac{x_\alpha}{l_\alpha^2}(u_3 - u_2) + \frac{y_\alpha}{l_\alpha^2}(v_3 - v_2) - \frac{\Omega}{2l_\alpha^2}(\psi_3 - \psi_2) \quad , \quad \gamma_{t\beta} = \frac{x_\beta}{l_\beta^2}(u_1 - u_3) + \frac{y_\beta}{l_\beta^2}(v_1 - v_3) - \frac{\Omega}{2l_\beta^2}(\psi_1 - \psi_3)$$
$$\text{and} \quad \gamma_{t\gamma} = \frac{x_\gamma}{l_\gamma^2}(u_2 - u_1) + \frac{y_\gamma}{l_\gamma^2}(v_2 - v_1) - \frac{\Omega}{2l_\gamma^2}(\psi_2 - \psi_1) \tag{58}$$

4.3.2 Transformation matrix

We are now in the position to construct matrix $\overline{\boldsymbol{\alpha}}_{\mathrm{N}}$ (eq. (20)) which is partitioned as follows:

$$\underset{(12\mathrm{x}18)}{\overline{\boldsymbol{\alpha}}_{\mathrm{N}}} = \begin{bmatrix} \underset{(6\mathrm{x}6)}{\overline{\boldsymbol{\alpha}}_{\mathrm{N}}^{11}} & \underset{(6\mathrm{x}6)}{\overline{\boldsymbol{\alpha}}_{\mathrm{N}}^{12}} & \underset{(6\mathrm{x}6)}{\overline{\boldsymbol{\alpha}}_{\mathrm{N}}^{13}} \\ \underset{(6\mathrm{x}6)}{\overline{\boldsymbol{\alpha}}_{\mathrm{N}}^{21}} & \underset{(6\mathrm{x}6)}{\overline{\boldsymbol{\alpha}}_{\mathrm{N}}^{22}} & \underset{(6\mathrm{x}6)}{\overline{\boldsymbol{\alpha}}_{\mathrm{N}}^{23}} \end{bmatrix} \tag{59}$$

A typical submatrix of eq. (59) is given by:

$$\underset{(6\mathrm{x}6)}{\overline{\boldsymbol{\alpha}}_{\mathrm{N}}^{11}} = \begin{bmatrix} . & . & . & . & . & . \\ x_\beta / l_\beta^{\,2} & y_\beta / l_\beta^{\,2} & . & . & . & -\dfrac{\Omega}{2l_\beta^2} \\ -x_\gamma / l_\gamma^{\,2} & -y_\gamma / l_\gamma^{\,2} & . & . & . & \dfrac{\Omega}{2l_\gamma^2} \\ . & . & . & . & . & . \\ . & . & . & -y_\beta / l_\beta & -x_\beta / l_\beta & . \end{bmatrix} \tag{60}$$

the others can be expressed similarly.

5 NUMERICAL TESTS

For the comparisons we used HKS ABAQUS v6.4 [14] (S3R general purpose triangle shell element, S4R general purpose quadrilateral shell element), MSC NASTRAN 2004 [15] (CTRIA3 general purpose triangle shell element, CTRIAR improved membrane triangle shell element, CQUAD4 general purpose quadrilateral shell element, CQUADR improved membrane quadrilateral shell element and CBEAM 2-node linear beam), standard TRIC and the improved TRIC elements.

5.1 Patch test (membrane mode)

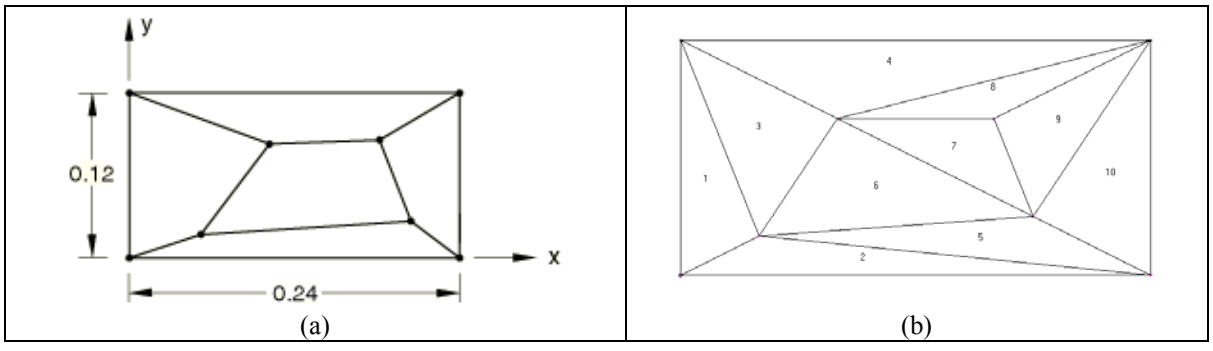

Figure 4: a) Model and b) FE mesh

The thickness of the membrane (Figure 4) is t = 0.001, while the material Modulus of Elasticity is $E = 1.0\times10^6$ and the Poisson ratio is $\nu = 0.25$. Out of plane displacement $U_z = 0$ is enforced for all nodes, while an in-plane displacement field is applied as a boundary condition for all the edge nodes: $U_x = 10–3((x+y/2)$, $U_y = 10\text{-}3(y+x/2)$.

The analytical solution is given by MacNeal, R.H., Harder, R.L. [16]: Stress $\sigma_{xx} = \sigma_{yy} = 1333$ and $\tau_{xy} = 400$ for all elements. Results for the improved TRIC element are: $\sigma_{xx} = \sigma_{yy} = 1333.33$ and $\tau_{xy} = 400.00$ for all elements.

5.2 Cantilever beam under an end moment

The cantilever beam of Figure 5 is subjected to an end moment M = 100. The modulus of elasticity is set to E = 768 and the exact tip deflection according to the classical beam theory $\delta_{tip} = ML/(2EI)$ is 100. Regular meshes ranging from 32×2 to 2×2 are used. Each rectanglular mesh unit being composed of 2 equal triangles. For the TRIC elements, 2 isotropic layers with equal height were used for every triangle. The element aspect ratios (γ) vary from 1:1 through 16:1. The root clamping conditions are shown in Figure 5.

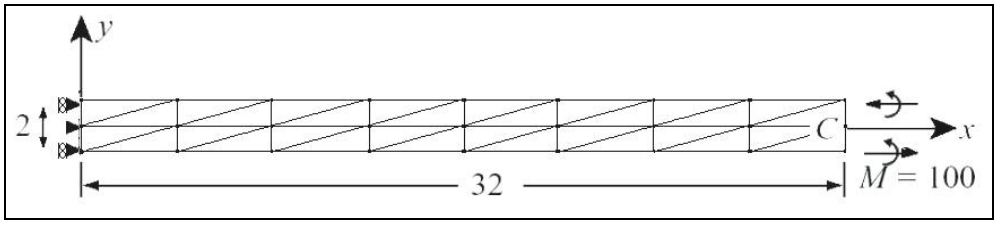

Figure 5: Cantilever beam under an end moment with 8×2 mesh (loading case a).

Two variations for the applied moment were used: a) two concentrated moments and two forces on opposite nodes, b) one concentrated moment in the middle node. Tables 1 to 2 report the computed tip deflections (*y* displacement at C for several element types and aspect ratio γ, for loading cases a, b and c, respectively. It can be seen that the performance of the improved TRIC outperforms the corresponding discretization with NASTRAN's triangle and is identical with Fellipa's improved plane stress triangular element and NASTRAN's quadrilateral element.

mesh (aspect ratio)	2x2 (γ = 16:1)	4x2 (γ = 8:1)	8x2 (γ = 4:1)	16x2 (γ = 2:1)	32x2 (γ = 2:1)
NASTRAN (Quads)	94.67	97.44	98.16	98.33	98.37
NASTRAN (Triangles)	1.25	4.82	15.83	36.62	54.31
TRIC	0.64	2.42	7.92	18.31	27.15
TRIC (improved)	101.32	101.22	101.0	100.58	100.07
Felippa [11]	99.99	99.99	99.99	99.96	100.07

Table 1: Cantilever beam computed tip deflections (*y* displacement at C) for loading case a

mesh (aspect ratio)	2x2 (γ = 16:1)	4x2 (γ = 8:1)	8x2 (γ = 4:1)	16x2 (γ = 2:1)	32x2 (γ = 2:1)
NASTRAN (Quads)	93.15	98.33	99.65	99.99	100.10
TRIC	0.00	0.00	0.00	0.00	0.00
TRIC (improved)	101.33	101.26	101.06	100.67	100.27

Table 2: Cantilever beam computed tip deflections (*y* displacement at C) for loading case b

5.3 Shear wall under bending or membrane loading

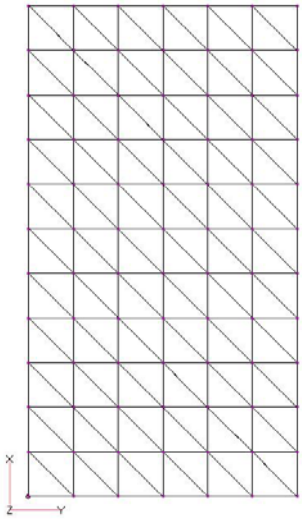

a)

Geometry of the wall:
Width l=5m, height h=9.2m and thickness t=0.4m

Material:
Modulus of elasticity: E = 32 GPa
Poisson ratio: ν = 0.30

Constraints:
Fully constrained at the base of the wall.

Mesh:
Structured mesh (6x11). Element width 0.83 m.

b)

Figure 6: a) FE mesh and b) model properties

In this example (Figure 6), the TRIC results are compared to a beam model results. In order to calculate the axial force, shear force and bending moment along a given section of the model, the finite element results are integrated along that section. Two different load cases were examined.

5.3.1 Behavior under shear force

A total shear load Fy = -70 is applied at the corresponding section on the top nodes (x = 9.2m) and is distributed in 7 nodal forces (Fy = 10KN each). A cantilever beam with force Fy at the top yields shear force distribution: Vy = Fy and bending moment distribution: Mz = Fy*(9.2-x). Three sections along the height of the shear wall were monitored: at the base (x=0.45m), at the middle (x=4.6m) and at the top (x=8.8m) of the wall.

Table 3 reports the results of the stress resultants for the three characteristic sections. It is obvious that both basic TRIC and improved TRIC exhibit the same results as the beam theory since both elements are satisfying the external work principal. Their difference though, is shown in the distribution of the calculated N_{xx} forces at the base section along the width of the shear wall (Figure 7). The improved TRIC element's force field presents no more than 5% deviation from the beam's theory field, while the basic TRIC differs up to 35%.

section	**Base**			**Middle**			**Top**		
	Vy	**Nx**	**Mz**	**Vy**	**Nx**	**Mz**	**Vy**	**Nx**	**Mz**
Analytical solution	-70.00	0.00	612.50	-70.00	0.00	321.30	-70.00	0.00	29.40
TRIC (improved)	-69.58	0.43	620.18	-70.02	1.09	327.61	-70.67	1.76	33.48
TRIC	-71.05	-0.21	594.42	-69.38	2.52	315.65	-69.96	1.95	31.89

Table 3: Shear wall under shear force. Stress resultants under characteristic sections.

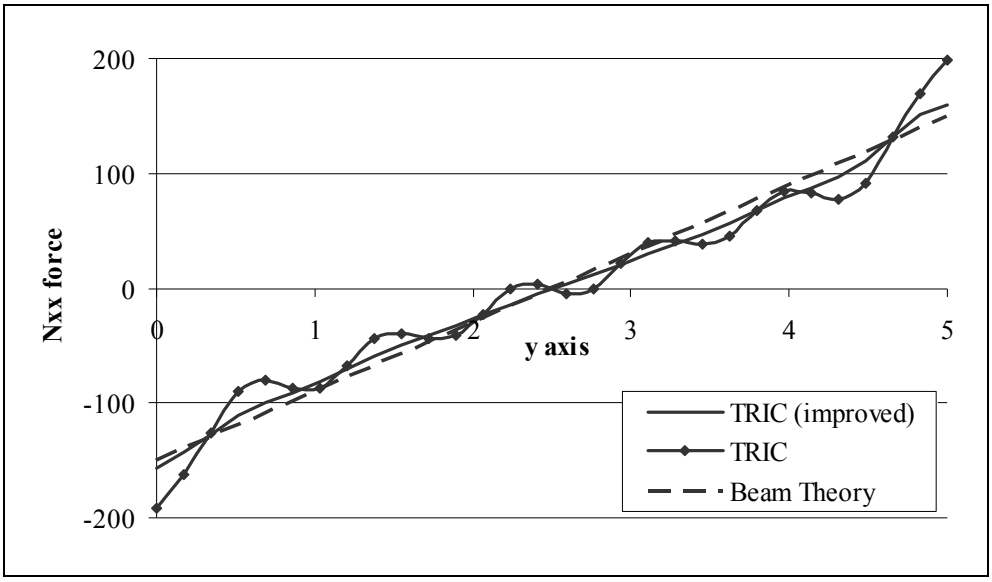

Figure 7: Shear wall under shear force. Calculated N_{xx} force along its width at the base section (x=0.45m).

Furthermore, the correct implementation of the drilling degrees of freedom in the improved TRIC can be seen from the amounts of consumed energy per natural mode. Figure 8 presents the consumed energy due to axial straining modes (eq. (10)) and due to azimuth rotational modes (eq. (13)) in the base of the wall. As expected (section 2.5.1) the basic TRIC presents no tuning of the azimuth modes and all energy is consumed by the axial modes.

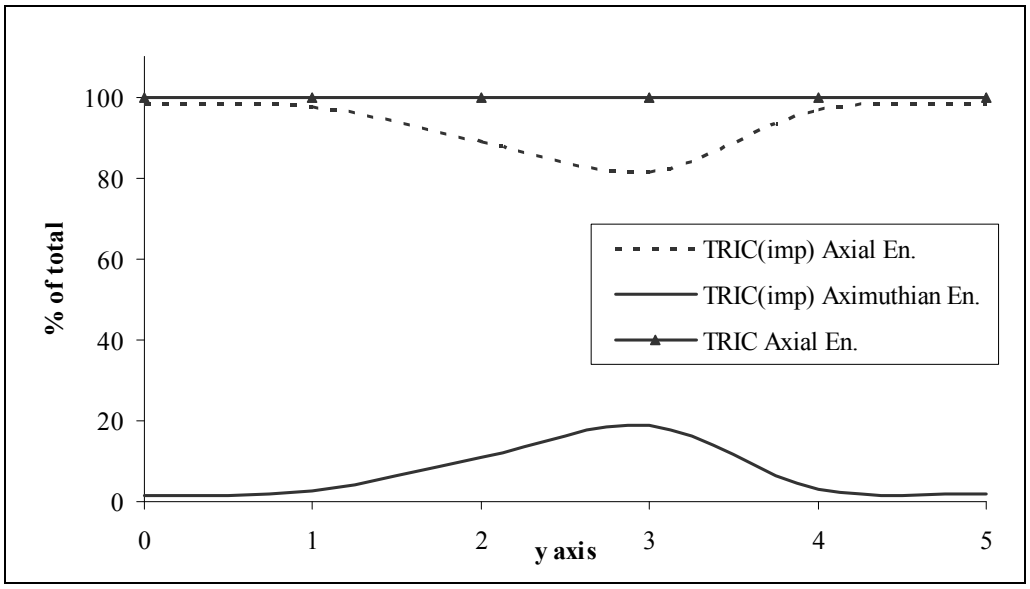

Figure 8: Shear wall under shear force. Consumed natural transformation energy along its width at the base section (percentage related to total energy).

5.3.2 Behavior under compression

A total axial load Fx = -70kN is applied at the corresponding section on the top nodes (x = 9.2m) and is distributed in 7 nodal forces (Fx = -10 each). Again three sections along the height of the shear wall were monitored as before.

Table 4 reports the results from section integration of finite element forces. Both basic TRIC and improved TRIC exhibit the same results as the beam theory, however the distribu-

tion of N_{xx} along the width of the shear wall differs substantially. The distribution of N_{xx} of the basic TRIC is far from the expected field (Figure 9).

section	Base		Middle		Top	
	Nx	Mz	Nx	Mz	Nx	Mz
Analytical solution	-70.00	0.00	-70.00	0.00	-70.00	0.00
TRIC (improved)	-70.04	0.37	-70.04	0.12	-70.84	-0.03
TRIC	-70.09	-0.92	-70.03	0.17	-70.58	-0.11

Table 4: Shear wall under compression. Stress resultants under characteristic sections.

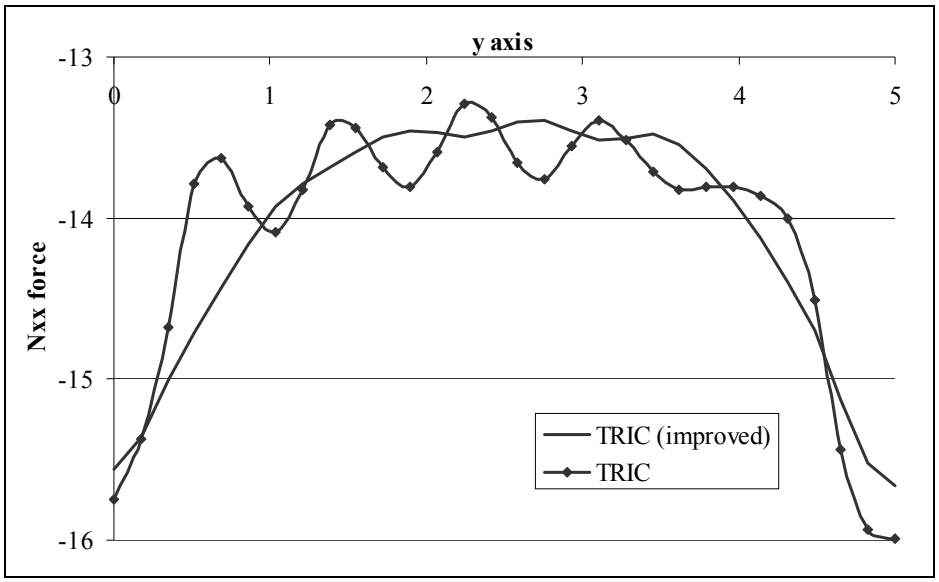

Figure 9: Shear wall under compression. Calculated Nxx force along its width at the base section (x=0.45).

5.4 Connection of shells with beam linear elements – Combined bending and mebrane loading

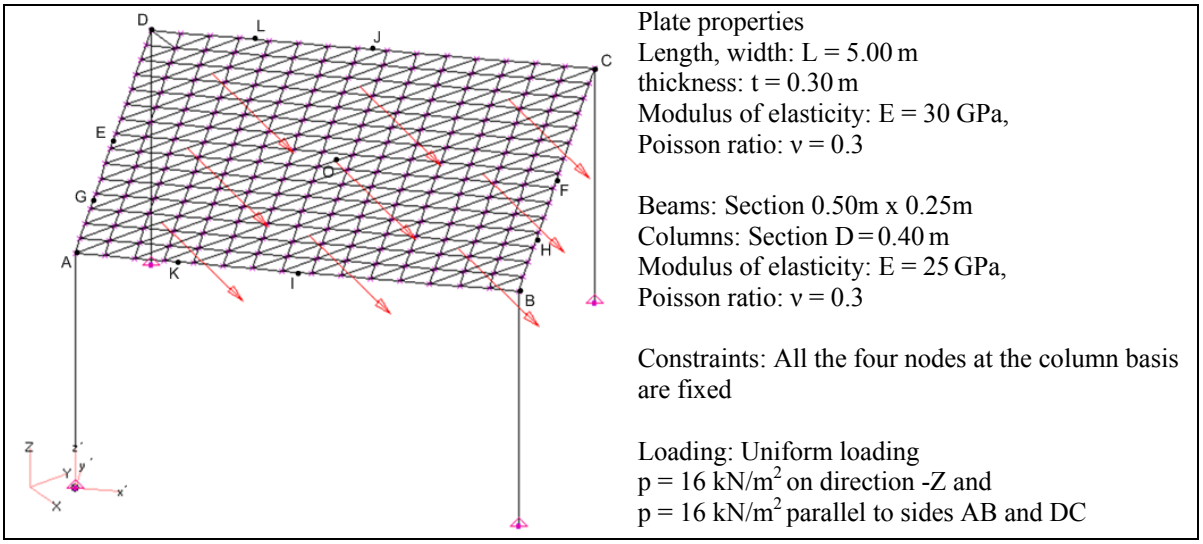

Figure 10: FE mesh and model properties for example 5.4

Mesh

Shell elements: 15x15 quad elements, the mesh for the triangular elements is obtained from the one for quad elements, by dividing each quad into two triangles.

Beams: Each structural beam is divided into 15 linear beam elements (in accordance with the mesh of the shell elements).

5.4.1 Results for shell elements

The results from the isoparametric shell elements for general use CQUAD4 (4-noded) and CTRIAR (improved triangular) of the program MSC-NASTRAN are used as benchnmarks.

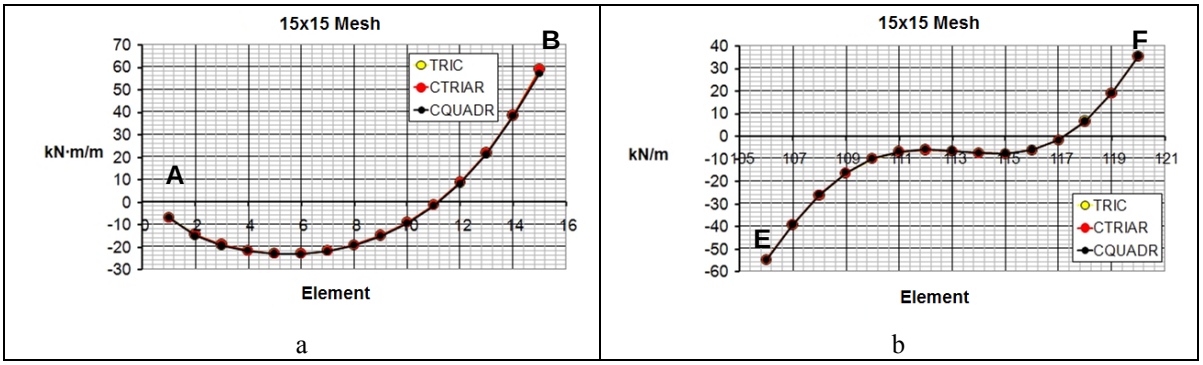

Figure 11: a) Bending moment $M_{x'x'}$ along the side AB and b) Force $F_{y'y'}$ along the side EF.

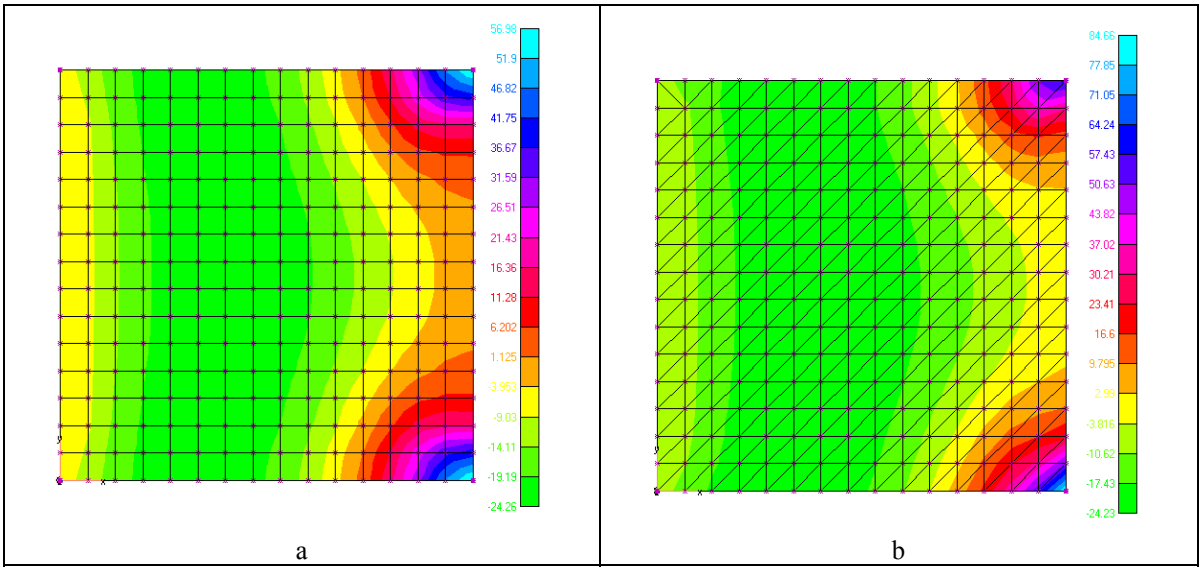

Figure 12: a) Bending moment $M_{x'x'}$ (CQUADR elements) and b) Bending moment $M_{x'x'}$ (TRIC elements).

5.4.2 Results for beam elements

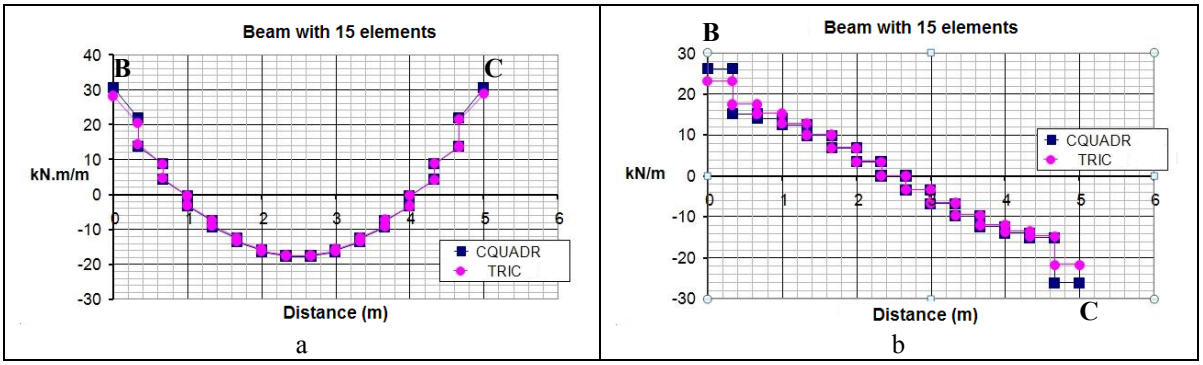

Figure 13: a) Bending moment M on beam BC and b) Shear force Q on beam BC.

There were small or negligible differences between the results of the analysis with TRIC and MSC-NASTRAN.

5.5 Plane frame with shear wall

The plane frame model of Figure 14 consists of a shear wall (height 9 m, width 2.5 m and thickness 0.25 m), three horizontal beams of 5 m length (0.5 m height and 0.25 m width, orthogonal section) and three columns of 3m height each (0.50 m rectangular section). It consists of isotropic material with elastic modulus equal to 30 GPa and Poisson ration equal to 0.20. All base nodes are fully constrained and three concentrated forces of magnitude 20 kN, 40 kN and 60 kN are applied on the center of the shear wall at heights 3 m, 6 m and 9 m, respectively.

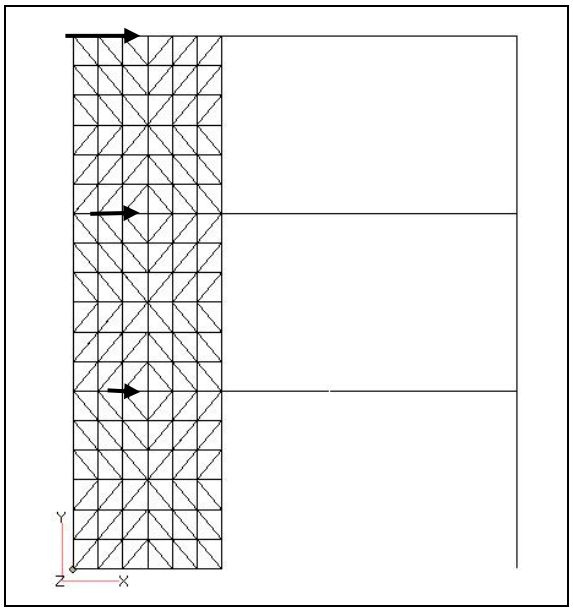

Figure 14: Plane frame with shear wall.

In all the analyses the shear wall was modeled with shell elements (TRIC (Improved), TRIC and the CQUAD4 quadrilaterals of MSC-NASTRAN), while beam elements were used for the beams and the columns. The TRIC element mesh is shown in the figure, while the rectangular mesh was composed of two equal triangles for every quadrilateral element.

In this test example, the TRIC element's ability to fully interact with beam elements is tested. Specifically, the connection between the shell's element azimouthian stiffness term and

the beam element's bending term was investigated. The reported bending moment of the beam elements for the improved TRIC, TRIC and MSC-NASTRAN, is presented in Figure 15.

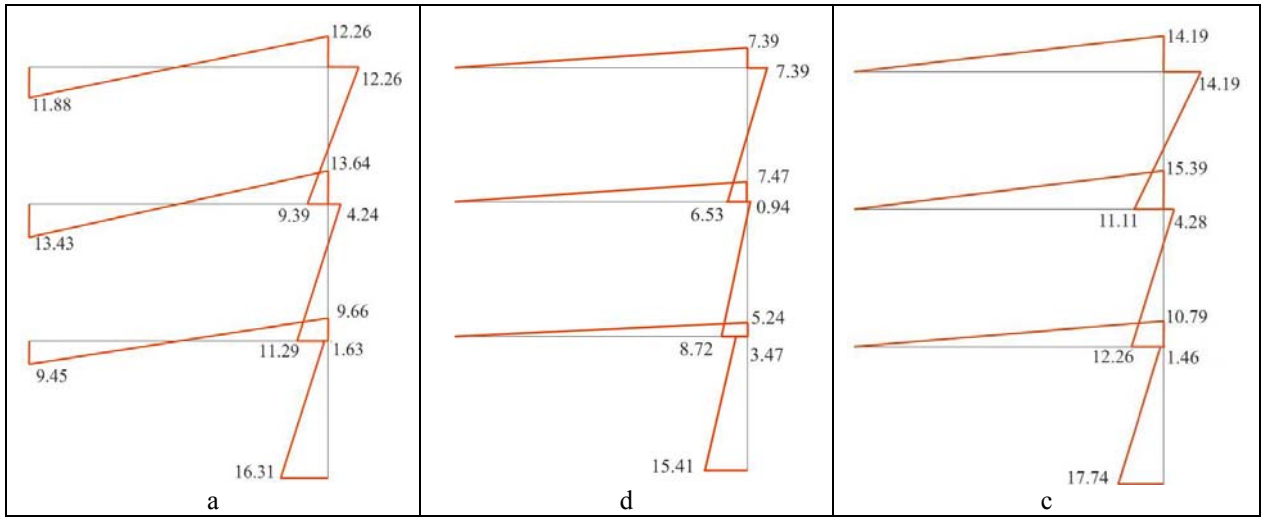

Figure 15: Bending moment of beam elements. a) shear wall discretized with improved TRIC elements b) shear wall discretized with TRIC elements c) shear wall discretized with MSC-NASTRAN quads

We can see that the improved TRIC shell element is capable of transmitting bending moment to the beams, through the azimuthian degree of freedom, while the CQUAD4 and TRIC elements of MSC-NASTRAN fail (there is no bending moment in the left corner of beams).

5.6 Single bay frame simulated with shell elements

The single bay model frame of Figure 16 consists of isotropic material, I shaped cross sections for both the columns and the beam. The beam web is perforated in two positions with elliptical holes. The geometry of these structures demands a more detailed simulation with shell finite elements, in order to capture the true deformation and stress patterns of the beam and columns.

The columns height is 220 and the beam length is 300. For the columns hw = 24 (web height), hf = 18 (flange height) and the thickness for both flange and web is 6. For the beam hw = 20 (web height), hf = 13 (flange height) and the thickness for both flange and web is 5. The Modulus of elasticity is E = 28 and the Poisson ratio is $\nu = 0.20$.

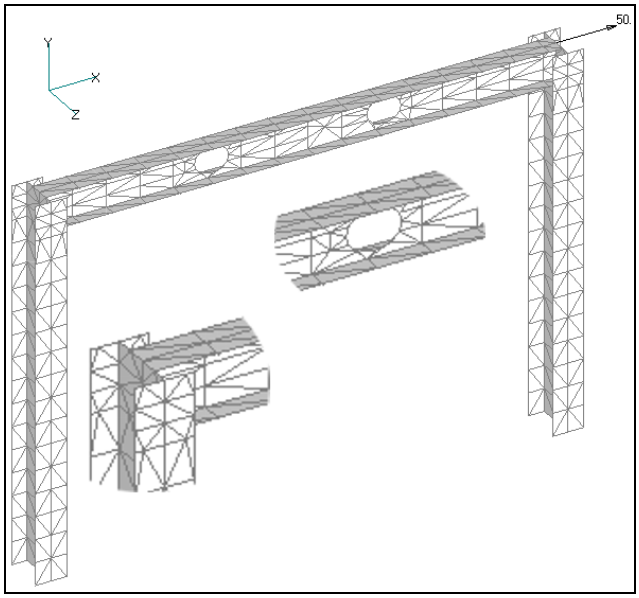

Figure 16: Single bay frame (433 nodes, 718 elements).

5.6.1 Static Loading

The structure is fully constrained in the bottom of the two columns and a concentrated force of magnitude 50 along the x direction was applied at the center top node of the right column (Figure 16). Two different analyses were conducted with MSC-NASTRAN quadrilateral elements. The first one with 550 elements and 648 nodes and the resulting tip deflection was found 160.49, while the second was performed with 1982 elements and 2168 nodes and its tip deflections was found 161.81.

Table 5 reports the computed tip deflections (x displacement at the node where the force was applied) for several element types and 6 different meshes. It can be seen that the improved TRIC behaves like the quadrilateral elements in terms of accuracy at the expense of require more elements to achieve the same performance. However, due to improved formulation aspects of TRIC, the computational afford is less than the corresponding effort by the quad elements for the same accuracy.

	Nodes	Elements	ABAQUS (Triangles)	NASTRAN (Triangles)	TRIC	TRIC (improved)	NASTRAN (Quads)
Triangles	**253**	**408**	45.40	49.63	49.09	146.03	-
	330	**540**	70.70	75.36	75.13	151.40	-
	363	**598**	72.60	76.90	76.79	153.67	-
	433	**718**	93.10	97.44	97.65	155.62	-
	658	**1108**	97.00	100.68	101.09	158.70	-
	1726	**2970**	119.00	120.09	121.40	160.11	-
Quads	**648**	**550**	-	-	-	-	160.49
	2168	**1982**	-	-	-	-	161.81

Table 5. Single bay frame computed tip deflections (x displacement at the node where the force was applied)

5.6.2 Elastoplastic Analysis

The material is perfectly plastic with yield stress $\sigma_y = 27$. In Figure 17 the results obtained for the models with 550 quadrilaterals elements and with 598 triangle elements are presented. The results confirm the superiority of the improved TRIC compared to the other triangular

elements while retaining its advantages over quadrilateral elements in terms of computational efficiency.

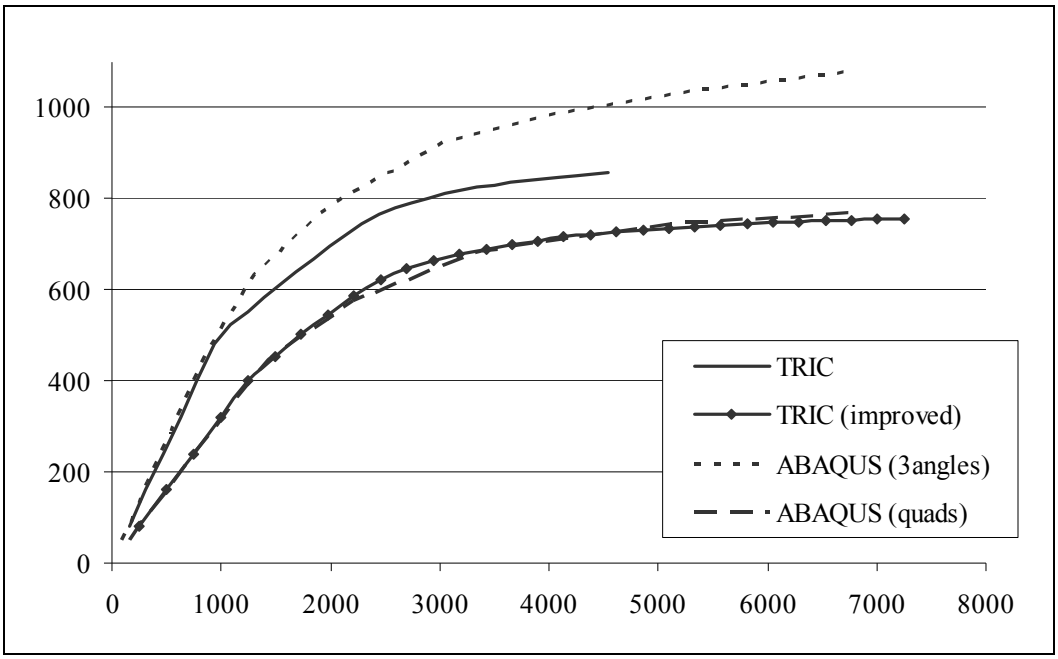

Figure 17: Single bay frame load-displacement curve of elastoplastic analysis (598 triangle elements and 550 quadrilateral elements).

6 CONCLUSIONS

From the above examples a number of concluding remarks can de drawn regarding the TRIC element and the proposed improvement. The standard TRIC element is very stiff and incapable to compute the exact deformation, when the membrane behavior is predominant, while finer meshes converge rather slowly to the correct solution. The improved TRIC exhibited substantially enhanced behavior compared to its original version. It is able to converge to the exact solution with coarse meshes as well as with distorted elements (aspect ratio 16:1).

Both stress and displacement fields of the improved element exhibits similar results compared either to analytical solutions or to those obtained with quadrilateral shell elements of commercial finite element programs. However, the computational cost for achieving the same accuracy is reduced due to the analytical computation of the elements stiffness matrix. In the test cases where section integration of the element's internal forces field was performed, the results were identical to the ones obtained by the exact beam theory.

The fifth example was a test bed for the behavior of the element in the case of connecting a beam element in shell's azimouthian rotational degree of freedom. In this case the beam element’s bending moment is computed through the shell’s azimouthian stiffness terms. The last example was a test bed for the behavior of the improved element in all kinds of modes (membrane, bending and shear). For this plane frame, the mesh was unstructured with elements of arbitrary aspect ratio resulting in a very distorted mesh. The improved TRIC exhibits excellent performance in both linear and elastoplastic analysis.

The improved TRIC response was substantially improved compared to both triangular and quadrilateral elements considered. In all the examples presented as well as of other conducted by the authors [17] the improved TRIC exhibited fast convergence to the correct solution compared to other general purpose shell elements.

ACKNOWLEDGEMENTS

The present work was carried out under the wing of the Meter 8.3 of the Operational Programme "Competitiveness" (3rd Community Support Programme) funded by the European Union (75%), the Greek Government [General Secretariat for Research and Technology of the Ministry of Development] (25%) and Private founds.

The support of the "John Argyris International Centre for Computer Applications in Engineering" is greatly acknowledged. The second author also acknowledges the support of the "John Argyris Foundation".

REFERENCES

[1] J.H. Argyris, L. Tenek, L. Olofsson, TRIC: a simple but sophisticated 3-node triangular element based on 6 rigid body and 12 straining modes for fast computational simulations of arbitrary isotropic and laminated composite shells. *Comp. Meth. Appl. Mech. Engrg.*, **145**, 11-85, 1997.

[2] J.H Argyris, M. Papadrakakis, C. Apostolopoulou, S. Koutsourelakis, The TRIC shell element: theoretical and numerical investigation. *Comp. Meth. Appl. Mech. Engrg.,* **182**, 217-245, 2000.

[3] J.H. Argyris, L. Tenek, M. Papadrakakis, C. Apostolopoulou, Postbuckling performance of the TRIC natural mode triangular element for isotropic and laminated composite shells. *Comp. Meth. Appl. Mech. Engrg.*, **166**, 211-231, 1998.

[4] A. Gisakis, M. Papadrakakis, L. Karapitta (2005), Improving the performance of the TRIC shell element. *5th International Congress on Computational Mechanics (GRACM 05)*, Limassol, Cyprus, June 29-30, 2005.

[5] J.H. Argyris, H. Balmer, J.St. Doltsinis, P.C. Dunne, M. Haase, M. Muller, W.D. Scharpf , Finite element method – the natural approach. *Comp. Meth. Appl. Mech. Engrg.*, **17/18**, 1-106, 1979

[6] M.J. Turner, R.W. Clough, H.C. Martin, L.J. Topp, Stiffness and deflection analysis of complex structures. *J. Aero. Sci.*, **23**, 805–824, 1956.

[7] J.H. Argyris, M. Papadrakakis, L. Karapitta, Elasto-plastic analysis of shells with the triangular element TRIC. *Comp. Meth. Appl. Mech. Engrg.* **191**, 3613-3636, 2002.

[8] J.H. Argyris, H. Balmer, M. Kleiber, U. Hindenlang, Natural description of large inelastic deformation for shells of arbritrary shape-application of TRUMP element. *Comp. Meth. Appl. Mech. Engrg*, **22**, 361-389, 1980.

[9] J.H. Argyris, D.W. Scharpf, J.B. Spooner, Technical Report, No. 46, 1968, University of Stuttgart, Germany.

[10] P.G. Bergan, C.A. Felippa, A triangular membrane element with rotational degrees of freedom. *Comp. Meth. Appl. Mech. Engrg.*, **50**, 25-69, 1685.

[11] C.A. Felippa, A study of optimal membrane triangles with drilling freedoms. *Comp. Meth. Appl. Mech. Engrg.*, **192**, 2125-2168, 2003.

[12] C.A Felippa, C. Militello, Membrane triangles with corner drilling freedoms. II. The ANDES element. *Finite Elements Anal. Des.*, **12**, 189-201, 1992.

[13] C. Militello, C.A. Felippa, The first ANDES elements: 9-dof plate bending triangles. *Comp. Meth. Appl. Mech. Engrg.*, **93**, 217-246, 1991.

[14] ABAQUS, Inc. HKS ABAQUS v6.4, Documentation manual (electronic book version).

[15] MSC-NASTRAN 2004, Reference manual (electronic book version).

[16] R.H. MacNeal, R.L. Harder, A proposed standard set of problems to test finite element accuracy. *Finite Elements in Analysis and Design*, **1**, 3-20, 1985.

[17] P. Tsirigas, A. Gisakis, V. Plevris, M. Papadrakakis, Evaluation and Verification of the TRIC shell element. *6th International Congress on Computational Mechanics (GRACM 06)*, Thessaloniki, Greece, June 19-21, 2008.